EINDHOVEN UNIVERSITY OF TECHNOLOGY

Translational and rotational friction on a colloidal rod near a wall

Citation for published version (APA):
Padding, J. T., & Briels, W. J. (2010). Translational and rotational friction on a colloidal rod near a wall. *Journal of Chemical Physics*, *132*(5), 054511-1/8. Article 054511. https://doi.org/10.1063/1.3308649

DOI:
10.1063/1.3308649

Document status and date:
Published: 01/01/2010

Document Version:
Publisher's PDF, also known as Version of Record (includes final page, issue and volume numbers)

Please check the document version of this publication:

• A submitted manuscript is the version of the article upon submission and before peer-review. There can be important differences between the submitted version and the official published version of record. People interested in the research are advised to contact the author for the final version of the publication, or visit the DOI to the publisher's website.
• The final author version and the galley proof are versions of the publication after peer review.
• The final published version features the final layout of the paper including the volume, issue and page numbers.

Link to publication

General rights
Copyright and moral rights for the publications made accessible in the public portal are retained by the authors and/or other copyright owners and it is a condition of accessing publications that users recognise and abide by the legal requirements associated with these rights.

• Users may download and print one copy of any publication from the public portal for the purpose of private study or research.
• You may not further distribute the material or use it for any profit-making activity or commercial gain
• You may freely distribute the URL identifying the publication in the public portal.

If the publication is distributed under the terms of Article 25fa of the Dutch Copyright Act, indicated by the "Taverne" license above, please follow below link for the End User Agreement:

www.tue.nl/taverne

Take down policy
If you believe that this document breaches copyright please contact us at:

openaccess@tue.nl

providing details and we will investigate your claim.

Download date: 04. Oct. 2023

The Journal of Chemical Physics

Translational and rotational friction on a colloidal rod near a wall

J. T. Padding and W. J. Briels

Citation: J. Chem. Phys. **132**, 054511 (2010); doi: 10.1063/1.3308649
View online: http://dx.doi.org/10.1063/1.3308649
View Table of Contents: http://jcp.aip.org/resource/1/JCPSA6/v132/i5
Published by the American Institute of Physics.

Related Articles

A Smoluchowski model of crystallization dynamics of small colloidal clusters
J. Chem. Phys. 135, 154506 (2011)

Reaction coordinates for the crystal nucleation of colloidal suspensions extracted from the reweighted path ensemble
J. Chem. Phys. 135, 154110 (2011)

Short-time rheology and diffusion in suspensions of Yukawa-type colloidal particles
J. Chem. Phys. 135, 154504 (2011)

Communication: A packing of truncated tetrahedra that nearly fills all of space and its melting properties
J. Chem. Phys. 135, 151101 (2011)

Re-entrant behavior in dynamics of binary mixtures of soft hybrid nanocolloids and homopolymers
J. Chem. Phys. 135, 134901 (2011)

Additional information on J. Chem. Phys.

Journal Homepage: http://jcp.aip.org/
Journal Information: http://jcp.aip.org/about/about_the_journal
Top downloads: http://jcp.aip.org/features/most_downloaded
Information for Authors: http://jcp.aip.org/authors

ADVERTISEMENT

Downloaded 21 Oct 2011 to 131.155.151.93. Redistribution subject to AIP license or copyright; see http://jcp.aip.org/about/rights_and_permissions

Translational and rotational friction on a colloidal rod near a wall

J. T. Padding[a)] and W. J. Briels
Computational Biophysics, University of Twente, P.O. Box 217, 7500 AE Enschede, The Netherlands

(Received 16 November 2009; accepted 14 January 2010; published online 5 February 2010)

We present particulate simulation results for translational and rotational friction components of a shish-kebab model of a colloidal rod with aspect ratio (length over diameter) $L/D=10$ in the presence of a planar hard wall. Hydrodynamic interactions between rod and wall cause an overall enhancement of the friction tensor components. We find that the friction enhancements to reasonable approximation scale inversely linear with the closest distance d between the rod surface and the wall, for d in the range between $D/8$ and L. The dependence of the wall-induced friction on the angle θ between the long axis of the rod and the normal to the wall is studied and fitted with simple polynomials in cos θ. © *2010 American Institute of Physics*. [doi:10.1063/1.3308649]

I. INTRODUCTION

A particle suspended in a fluid, moving in the vicinity of a stationary wall, feels a viscous drag force that is larger than the viscous drag it would experience in the bulk fluid.[1–3] This may intuitively be understood by considering the special case of a particle moving toward (away from) a wall: fluid needs to be squeezed out (sucked into) the gap between the particle and the wall. Even when the particle is relatively far away from the wall, the hindering effects of the wall are still felt through the long-ranged hydrodynamic interactions. This has important consequences for practical applications where flow and time are issues. Especially for microfluidic applications,[4] where large surface to volume ratios are encountered, it is important to understand the fundamentals of near-wall dynamics.

When dealing with colloidal particles, random forces should also be taken into account.[5] The random forces are caused by temporary imbalances in the collisions with the solvent molecules and lead to diffusive (Brownian) motion of the colloidal particles. The diffusive behavior of nanometer to micrometer sized particles near walls is essential for the transient kinetics of phenomena such as wetting and particle deposition on a substrate.[6]

The (anisotropic) diffusion tensor $\mathbf{D}$ of a colloidal particle is related to the anisotropic friction tensor $\boldsymbol{\Xi}$ by the generalized Einstein relation $\mathbf{D}=k_BT\boldsymbol{\Xi}^{-1}$, where k_BT is the thermal energy. The friction tensor in the presence of a stick boundary wall is difficult to obtain theoretically. Analytical expressions in the creeping flow limit (applicable to colloidal particles) are known, but are limited to the case of a spherical particle[2,7] or to a nonspherical particle whose major (hydrodynamic) axes are aligned with the wall and which is far removed from the wall.[3,8] In the general case, particles are not aligned with the wall and/or may not be far removed from it. One then has to resort to experiment or numerical evaluation to obtain the friction or diffusion tensor.

Experimentally, optical microscopy,[9–12] total internal reflection microscopy,[13,14] and evanescent wave dynamic light scattering (EWDLS)[6,15,16] have been used to determine the diffusivity of particles near a wall. The latter two experimental techniques use the short penetration depth of an evanescent wave under total internal reflection conditions, where in EWDLS this is combined with dynamic light scattering. In EWDLS, the different components of the diffusion tensor may be obtained from the intensity time autocorrelation, but this requires several careful theoretical interpretations.[16]

Numerical evaluation of the friction on a particle can be performed in several ways: by numerical summation of the forces due to a large number of Stokeslets distributed over the walls and surfaces of the particles,[5,17] possibly including image singularities to efficiently capture the effect of a planar wall,[18–20] or by a multipole expansion of the force densities induced on the spheres, also with an image representation to account for a planar wall.[21,22]

In this paper, we will present an alternative way to determine the friction on a colloidal particle, using molecular dynamics simulations, which explicitly include the solvent particles. Because of the large difference in length scales between a colloidal particle and a solvent molecule, it is impossible to perform such simulations in full atomistic detail. Some form of coarse-graining is necessary. Here we choose the stochastic rotation dynamics (SRD) method to effectively represent the solvent.[23] The solvent interacts with walls and colloidal particles through excluded volume interactions.[24–26] Using this approach, we determine the friction on a shish-kebab model of a rod of aspect ratio 10, i.e., ten touching spheres on a straight line, as a function of distance to and angle (θ) with a planar wall. We will show that the functional dependence of the wall-induced friction enhancement can be reasonably well described by the inverse of the closest distance d between rod surface and the wall (for d in the range between one eighth the rod diameter and the rod length), and an angular dependence which may be expressed as a simple polynomial in cos θ. These results serve as a first example to show how SRD simulations may be used to determine the friction on particles of nontrivial shape in a nontrivial orientation with respect to confining boundaries.

[a)]Electronic mail: j.t.padding@gmail.com.

 © 2010 American Institute of Physics

Downloaded 21 Oct 2011 to 131.155.151.93. Redistribution subject to AIP license or copyright; see http://jcp.aip.org/about/rights_and_permissions

Stokesian dynamics codes, such as those developed by Swan and Brady[20] and Cichocki *et al.*[21] and Ekiel-Jeżewska *et al.*,[22] have other sophisticated methods to determine the friction tensor. The results from such methods are generally more precise (if sufficient care is taken in its implementation and choice of parameters) than those from SRD simulations because in SRD the solvent dynamics is stochastic and the resolution seems to be limited by the collision cell size. However, as we will show, in practice, the resolution is better than a collision cell size, and the influence of stochasticy can be severely reduced by taking long time averages, leading to an acceptable precision for making predictions. The biggest advantage of SRD over Stokesian dynamics is the extreme simplicity of the implementation of the SRD method when nontrivial shapes and complex confining boundaries are involved. In Stokesian dynamics methods, one has to deal with complicated multipole expansions and image representations. If the embedded particle shape is nontrivial or if the confining boundaries are not planar but more complex, they have to be represented by assemblies of different sized spheres. In contrast, in SRD, being essentially a molecular dynamics technique with a simple additional rule for momentum exchange, all that is needed is a rule to determine when a solvent point particle overlaps with the embedded particle or wall. The SRD method then automatically takes care of all hydrodynamic interactions between complex shapes.

This paper is organized as follows. In Sec. II, we give details of the simulations method and the constraint technique by which we determine the hydrodynamic friction. In Sec. III, we validate the method by comparing simulations of a sphere near a planar wall with known analytical expressions. Then in Sec. IV, we study the friction on a rod. In Sec. V, we conclude.

II. METHOD

A. Simulation details

In SRD,[23] a fluid is represented by N_f ideal particles of mass m. After propagating the particles for a time δt_c, the system is partitioned in cubic cells of volume a_0^3. The velocities relative to the center-of-mass velocity of each separate cell are rotated over a fixed angle α around a random axis. This procedure conserves mass, momentum, and energy and yields the correct hydrodynamic (Navier–Stokes) equations, including the effect of thermal noise.[23] The fluid particles only interact with each other through the rotation procedure, which can be viewed as a coarse-graining of particle collisions over time and space.

To simulate the colloidal spheres, we follow our earlier implementation described in Ref. 25. Throughout this paper, our results are described in units of SRD mass m, SRD cell size a_0, and thermal energy k_BT. The number density (average number of SRD particles per SRD cell) is fixed at $\gamma=5$, the rotation angle is $\alpha=\pi/2$, and the collision interval $\delta t_c=0.1t_0$, with time units $t_0=a_0(m/k_BT)^{1/2}$. This corresponds to a mean-free path of $\lambda_{\text{free}}\approx 0.1a_0$. In our units, these choices mean that the fluid viscosity takes the value $\eta=2.5m/a_0t_0$ and the kinematic viscosity is $\nu=0.5a_0^2/t_0$. The Schmidt number Sc, which measures the rate of momentum (vorticity) diffusion relative to the rate of mass transfer, is given by $\text{Sc}=\nu/D_f\approx 5$, where D_f is the fluid self-diffusion constant.[26–28] In a gas $\text{Sc}\sim 1$, momentum is mainly transported by moving particles, whereas in a liquid, Sc is much larger and momentum is primarily transported by interparticle collisions. For our purposes, it is only important that vorticity diffuses faster than the particles do.

Stochastic stick boundaries are implemented as described in Ref. 25. In short, SRD particles that overlap with a wall or sphere are bounced back into the solvent with tangential and normal velocities from a thermal distribution. The change of momentum is used to calculate the force on the boundary. We note that despite the fact that the boundaries are taken into account through stochastic collision rules, the *average* effect is that of a classical stick boundary as often employed in (Stokesian) continuum mechanics. Because we will determine frictions by taking long time averages, the average flow velocities close to the boundaries will be effectively zero in all directions. In this work, we set the sphere diameter to $D=8a_0$, which is sufficiently large to accurately resolve the hydrodynamic field to distances as small as $D/16$, as already shown in Refs. 25 and 26. The method will be validated here again by comparing the friction between a sphere and a wall with known expressions from hydrodynamic theory.

Walls are present at $z=0$ and $z=L_z$, i.e., the wall normal $\hat{\mathbf{n}}$ is in the z direction. Simulations containing a single sphere are performed in a box of dimensions $L_x=L_y=L_z=80a_0$, corresponding to $10D$ in each direction. Simulations containing a rod with its longest axis along $\hat{\mathbf{n}}$ are performed in a box of $10D\times 10D\times 20D$. All other rod simulations are performed in a box of dimensions $20D\times 10D\times 20D$. The latter boxes contain approximately 10^7 SRD particles. Note that the finite box dimensions imply that there will still be an important self-interaction of the rod with its periodic images. Larger boxes are computationally too expensive. In this work, we will assume that the dependence of the hydrodynamic friction on angle and distance to the wall is dominated by the presence of the wall itself and that self-interactions with periodic images lead to a simple overall multiplication factor of the friction.

All simulations were run for a time of $5\times 10^5 t_0$, i.e., 5×10^6 collision time steps. In CPU time, this corresponds to about 4 weeks on a modern single core processor. Such long run times are necessary to attain sufficient accuracy in the determination of the friction, the method of which is explained in the following paragraph.

B. Determination of the friction

The translational friction tensor $\boldsymbol{\Xi}$ transforms the translational velocity $\mathbf{v}$ of the center-of-mass of an object to the friction force $\mathbf{F}$ it experiences. Similarly, the rotational friction tensor $\mathbf{Z}$ transforms the rotational velocity $\boldsymbol{\omega}$ around the center-of-mass to the friction torque $\mathbf{T}$. In formula,

$$\mathbf{F}=-\boldsymbol{\Xi}\cdot\mathbf{v}, \tag{1}$$

Downloaded 21 Oct 2011 to 131.155.151.93. Redistribution subject to AIP license or copyright; see http://jcp.aip.org/about/rights_and_permissions

$$\mathbf{T} = -\mathbf{Z} \cdot \boldsymbol{\omega}. \tag{2}$$

In our simulations, the translational friction tensor is determined without actually moving the rod by measuring the time correlation of the constraint force $\mathbf{F}^c$ needed to keep the rod at a fixed position,[29,30]

$$\Xi_{\alpha\beta} = \frac{1}{k_B T}\int_0^\infty \mathrm{d}\tau \langle F_\alpha^c(t_0+\tau) F_\beta^c(t_0)\rangle_{t_0}, \tag{3}$$

where $\alpha, \beta \in \{x, y, z\}$ and the subscript to the pointy brackets indicates an average over many time origins t_0. Similarly, the rotational friction tensor is determined from the time correlation of the constraint torque $\mathbf{T}^c$ needed to keep the rod at a fixed orientation,

$$Z_{\alpha\beta} = \frac{1}{k_B T}\int_0^\infty \mathrm{d}\tau \langle T_\alpha^c(t_0+\tau) T_\beta^c(t_0)\rangle_{t_0}. \tag{4}$$

It is important to realize that there are two sources of friction on a large particle.[24] The first comes from the hydrodynamic dissipation in the fluid induced by motion of the particle and may be obtained by solving Stokes' equation, integrating the solvent stress over the surface of the particle. For translation of a sphere of diameter D in an infinite fluid, this yields the familiar (isotropic) friction $\xi_h = 3\pi\eta D$. The second contribution is the Enskog friction,[31,32] which is the friction that a large particle would experience if it were dragged through a nonhydrodynamic ideal gas, i.e., through a gas where the velocities of the particles are uncorrelated in space and time and distributed according to the Maxwell–Boltzmann law. For a heavy sphere with diffusing boundaries (which randomly scatter colliding particles according to the Maxwell–Boltzmann law) the translational Enskog friction is given by $\xi_e = \frac{2}{3}\sqrt{2\pi m k_B T}\gamma D^2(1+2\chi)/(1+\chi)$, where $\chi = 2/5$ is the gyration ratio. It has been confirmed[25,26,31–33] that the two sources of friction act in parallel, i.e., that the total friction ξ is given by

$$\frac{1}{\xi} = \frac{1}{\xi_h} + \frac{1}{\xi_e}. \tag{5}$$

For simplicity, a scalar friction is shown here, but these results apply equally well to each component of the friction tensor. The parallel addition may be rationalized as follows. When a large particle is forced to move through a sea of smaller particles, it can dissipate energy through two parallel channels: (1) by dragging itself through this sea of small particles, resulting in more large-small collisions or (2) by setting up a flow field in the solvent, at the expense of viscous dissipation in the solvent but with the advantage that the sea of gas particles is co-moving near its surface, resulting in less large-small collisions.

In a real (experimental) colloidal suspension, both the solvent density and the range of the colloid-solvent interaction are larger than simulated here, which is why at any given time many more solvent molecules are interacting with each colloid. This leads to an Enskog friction which is orders of magnitude larger than the hydrodynamic friction (it is important to note that for a hard sphere in a point particle fluid, the Enskog friction increases faster than the hydrodynamic friction with increasing sphere diameter, $\xi_e \propto D^2$ and $\xi_h \propto D$). Hence, for real mesoscopic particles, the total friction ξ is practically equal to the hydrodynamic friction ξ_h. In our simulations, the Enskog friction on one sphere is only approximately four times larger than the hydrodynamic friction.[26]

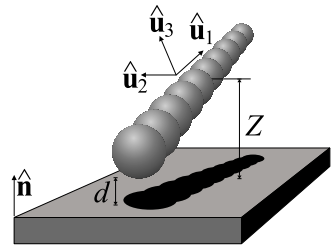

FIG. 1. Rod and wall geometry. Z is the height of the rod center-of-mass above the wall and d is the closest distance between the rod surface and the wall, which has its normal in the $\hat{\mathbf{n}}$ direction. The unit vector $\hat{\mathbf{u}}_1$ is along the long axis of the rod, $\hat{\mathbf{u}}_2$ is perpendicular to the rod and pointing parallel to the wall surface, and $\hat{\mathbf{u}}_3$ is perpendicular to the previous two. The angle θ is defined through $\hat{\mathbf{n}} \cdot \hat{\mathbf{u}}_1 = \cos\theta$.

In our simulations, we can easily determine the Enskog friction. In many ways, the hard-colloid and SRD fluid system is like a hard sphere system, in which case the general structural features of the force autocorrelation (or time dependent friction) are (a) an initial delta function contribution whose integral is the Enskog friction and (b) a slower contribution associated with correlated collisions and collective effects, which is negative for low and intermediate particle densities.[31] The Enskog friction can therefore be read off as the peak value in the running integral of Eq. (3), $\Xi_{\alpha\beta}(t) = (1/k_B T)\int_0^t \mathrm{d}\tau \langle F_\alpha^c(t_0+\tau) F_\beta^c(t_0)\rangle_{t_0}$, at very short times t. Note that for continuous interactions, there is no clear-cut separation as described here.[31] Applying the above procedure to the case of a sphere yields an Enskog friction which is in good agreement with theoretical prediction, as we will show in Sec. III. Equation (5) is then inverted to $\xi_h = 1/(1/\xi - 1/\xi_e)$ to obtain the hydrodynamic friction coefficient which would be measured for a particle with orders of magnitude higher Enskog friction.

C. Choice of system coordinates

Looking at Fig. 1, it is clear that the Cartesian coordinates x, y, and z may not be the most natural coordinates to use when considering the friction on a rod. In this section, we will introduce coordinates that are better adapted to the symmetry of the problem. We will show this for the case of the translational friction, but similar results will apply to the rotational friction.

By symmetry, given the orientation of the rod in the xz plane, the components Ξ_{xy} and Ξ_{yz} must be zero (and hence also Ξ_{yx} and Ξ_{zy}). The remaining four independent components are the diagonals and the xz component (which is equal to the zx component). Their relative importance in general depends on the orientation of the rod. In order to simplify this dependence as much as possible, we transform the friction tensors to a rod-based orthogonal coordinate system, defined as follows (see Fig. 1):

Downloaded 21 Oct 2011 to 131.155.151.93. Redistribution subject to AIP license or copyright; see http://jcp.aip.org/about/rights_and_permissions

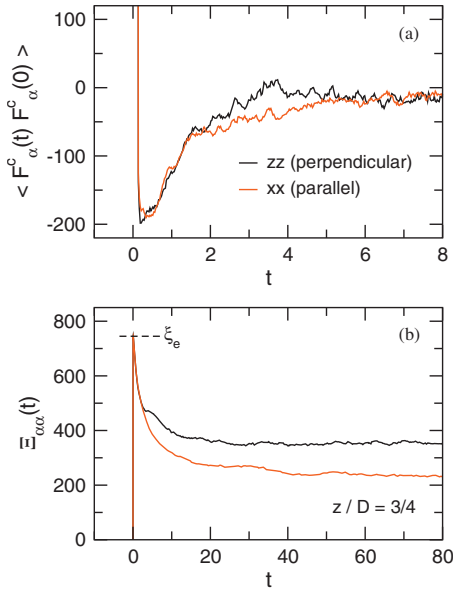

FIG. 2. (a) Autocorrelation of the constraint force needed to keep a sphere at fixed position $Z=3/4D$ above a wall. Forces perpendicular to the wall (zz) are shown in black and forces parallel to the wall (xx) in red. (b) Running integral of the data in (a) (divided by k_BT). The peak value at short times yields the Enskog friction (dashed line) ξ_e, which determines the short time self-diffusion of a colloid in a Brownian bath without hydrodynamic interactions. The total friction ξ is estimated from the long time limit of the running integral. The hydrodynamic friction ξ_h is obtained by applying Eq. (5).

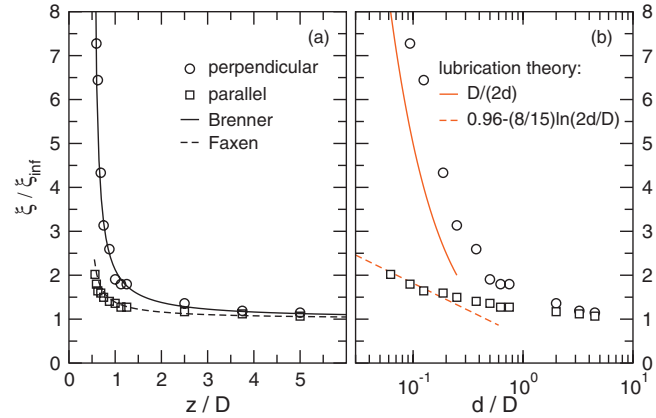

FIG. 3. (a) Hydrodynamic friction enhancement due to the presence of a wall as a function of normalized height Z/D of the sphere's center above the wall. Simulation results (circles and squares) are compared with theoretical expressions (black lines) for the friction for perpendicular motion toward and away from the wall, Eq. (15) (Ref. 2), and for motion parallel to the wall, Eq. (16) (Ref. 1). (b) Hydrodynamic friction enhancement as a function of normalized closest distance d/D, with $d=Z-D/2$, on a semilogarithmic scale. The simulation results (circles and squares) are compared with lubrication theory asymptotes (Refs. 2 and 7), which are valid for $d \ll D$ (red lines).

$$\hat{\mathbf{u}}_1 = \hat{\mathbf{u}}, \tag{6}$$

$$\hat{\mathbf{u}}_2 = \frac{\hat{\mathbf{n}} \times \hat{\mathbf{u}}}{|\hat{\mathbf{n}} \times \hat{\mathbf{u}}|}, \tag{7}$$

$$\hat{\mathbf{u}}_3 = \frac{\hat{\mathbf{u}} \times (\hat{\mathbf{n}} \times \hat{\mathbf{u}})}{|\hat{\mathbf{n}} \times \hat{\mathbf{u}}|}. \tag{8}$$

In short, $\hat{\mathbf{u}}_1$ is along the rod, $\hat{\mathbf{u}}_2$ is perpendicular to the rod but parallel to the wall, and $\hat{\mathbf{u}}_3$ is perpendicular to the previous two. If θ is the angle between the long axis of the rod and the wall normal ($\hat{\mathbf{n}} \cdot \hat{\mathbf{u}} = \cos\theta$), with $\theta \in [0, \pi/2]$, then the transformation matrix $\mathbf{U}$ between the Cartesian frame and this new coordinate system is given by

$$\mathbf{U} = \begin{bmatrix} \sin\theta & 0 & -\cos\theta \\ 0 & 1 & 0 \\ \cos\theta & 0 & \sin\theta \end{bmatrix}. \tag{9}$$

With this we can calculate the transformed friction tensor as

$$\tilde{\Xi} = \mathbf{U}^T \Xi \mathbf{U} = \begin{bmatrix} \xi_\parallel & 0 & \xi' \\ 0 & \xi_{\perp 1} & 0 \\ \xi' & 0 & \xi_{\perp 2} \end{bmatrix}, \tag{10}$$

where the friction components are given by

$$\xi_\parallel = \sin^2\theta \Xi_{xx} + 2\sin\theta\cos\theta \Xi_{xz} + \cos^2\theta \Xi_{zz}, \tag{11}$$

$$\xi_{\perp 1} = \Xi_{yy}, \tag{12}$$

$$\xi_{\perp 2} = \cos^2\theta \Xi_{xx} - 2\sin\theta\cos\theta \Xi_{xz} + \sin^2\theta \Xi_{zz}, \tag{13}$$

$$\xi' = \sin\theta\cos\theta(\Xi_{zz} - \Xi_{xx}) + (\sin^2\theta - \cos^2\theta)\Xi_{xz}. \tag{14}$$

It will turn out that the mixing term ξ' is small relative to the other terms.

III. VALIDATION: FRICTION ON A SPHERE NEAR A WALL

To validate our method, we first determine the friction on a single sphere as a function of its height z above a wall and compare with known theoretical expressions. We have determined the constraint force autocorrelations on a sphere of diameter $D=8a_0$ for a series of heights ranging from $Z/D=0.6$ to 5.0 in a cubic box of size $L=10D$ along each axis. An example for $Z/D=0.75$ (i.e., with a closest distance $d=0.25D$ between the wall and the bottom of the sphere) is given in Fig. 2(a) where we show both the perpendicular (zz) and parallel (xx) components. The structural features of the force autocorrelations are, as expected,[31] an initial delta function contribution, whose integral is the Enskog friction, and a slower contribution associated with correlated collisions and collective effects, which is negative for our relatively low particle density.

The running integral of the constraint force autocorrelation (divided by k_BT) is shown in Fig. 2(b). The peak value at short times measures 0.74×10^3 in simulation units, which is in good agreement with the expected Enskog friction of $\xi_e = 0.69 \times 10^3$. We note that the measured peak value of 0.74×10^3 was found consistently for all distances between sphere and wall. This confirms that the value of the Enskog friction is a local effect, unaffected by the geometry of the surroundings of the sphere.

After the Enskog peak, the running integrals converge slowly to their final values, in the particular case shown $\Xi_{zz}=0.35 \times 10^3$ and $\Xi_{xx}=0.23 \times 10^3$, but with other values for other distances between sphere and wall. Using the mea

Downloaded 21 Oct 2011 to 131.155.151.93. Redistribution subject to AIP license or copyright; see http://jcp.aip.org/about/rights_and_permissions

sured Enskog friction, we then calculate the perpendicular and parallel hydrodynamic frictions. For large values of Z/D, these hydrodynamic frictions converge to a value $\xi^{\infty} = 230 \pm 20$, which is in good agreement with the expected value of $\xi^{\text{theor}} = 3\pi\eta D/(1-1.45D/L) = 220$, where the factor between brackets takes into account finite system size effects.[26,34,35]

In Fig. 3(a), we plot the resulting perpendicular (circles) and parallel (squares) hydrodynamic frictions, normalized by ξ^{∞}, as a function of normalized height Z/D of the sphere's center above the wall. Clearly, the friction is enhanced greatly as the sphere comes nearer to the wall. A theoretical derivation for the perpendicular friction enhancement $\lambda_{\perp}$ was given in 1961 by Brenner,[2] with the result

$$\lambda_{\perp}(Z) = \frac{4}{3}\sinh\alpha \sum_{n=1}^{\infty} \frac{n(n+1)}{(2n-1)(2n+3)} \left[\frac{2\sinh((2n+1)\alpha) + (2n+1)\sinh(2\alpha)}{[2\sinh((n+1/2)\alpha)]^2 - [(2n+1)\sinh\alpha]^2} - 1 \right], \tag{15}$$

where $\alpha = \cosh^{-1}(2Z/D)$. Figure 3(a) shows this theoretical result as a solid line. There is no exact analytical expression for the parallel friction enhancement $\lambda_{\parallel}$. A commonly applied approximation due to Faxén,[1] which deviates less than 10% from the result of precise numerical calculations for $Z/D > 0.52$ and gives essentially the same results for $Z/D > 0.7$,[7] is the following:

$$\lambda_{\parallel}(Z) = \left[1 - \frac{9}{32}\frac{D}{Z} + \frac{1}{64}\left(\frac{D}{Z}\right)^3 - \frac{45}{4096}\left(\frac{D}{Z}\right)^4 - \frac{1}{512}\left(\frac{D}{Z}\right)^5 \right]^{-1}. \tag{16}$$

Figure 3(a) shows this expression as a dashed line. The simulation results for the friction enhancements are in good agreement with both theoretical expressions.

When the closest distance $d = Z - D/2$ is much smaller than the sphere diameter, i.e., when $d \ll D$, the Stokes equations can be solved asymptotically, leading to so-called lubrication forces.[2,7] For the perpendicular friction enhancement, the lubrication prediction diverges as the inverse closest distance,[2]

$$\lim_{d/D \to 0} \lambda_{\perp} = \frac{D}{2d}. \tag{17}$$

For the parallel friction enhancement, the lubrication prediction diverges logarithmically,[7]

$$\lim_{d/D \to 0} \lambda_{\parallel} \approx 0.9588 - \frac{8}{15}\ln\frac{2d}{D}, \tag{18}$$

where the constant 0.9588 has been determined by fitting to precise numerical calculations.[7] An interesting question is whether our simulations are able to reproduce these asymptotes. Lubrication forces are in essence a hydrodynamic effect and the SRD method in principle resolves fully the hydrodynamics, at least down to the scale of a cell size a_0. The resolution is even better than this because of the averaging effect of the applied random grid shift.[36]

Figure 3(b) shows the friction enhancements measured in the simulations and the lubrication predictions against the logarithm of d/D, thus emphasizing the behavior at small distances. We observe that our method predicts a perpendicular friction, which approaches the lubrication prediction (solid red line) from above, but does not yet reach this limit within the range of distances studied. The approach is quite slow, which is in agreement with the exact expression Eq. (15). The parallel friction approaches the lubrication prediction (dashed red line) from above too, but here the lubrication limit is reached already for $d/D < 0.1$, in agreement with observations by Goldman *et al.*[7]

The good agreement of our results with the theoretical predictions for a sphere, both at small and large distances, gives us confidence that the same method may also be applied to the case of a rod for which no theoretical predictions are known. In the remainder of this paper, we will focus on closest distances in the range of $D/8$ to $10D$. We will show that in this range of distances the wall-induced friction enhancement can be approximately described by additive contributions scaling linearly with D/d. We emphasize that this scaling is not exact, but serves to represent our measurements in a compact functional form which may be useful for future simulations. The similarity of the d^{-1} scaling with Eq. (17) is probably coincidental because lubrication theory generally is not valid at such large distances.

IV. FRICTION ON A ROD NEAR A WALL WITH $L/D=10$

A. Translational friction

A typical example of the running integral of the constraint force autocorrelation for a rod near a wall is given in Fig. 4. The diagonal components $\xi_{\parallel}$, $\xi_{\perp 1}$, and $\xi_{\perp 2}$ represent the magnitude of the friction antiparallel to the direction of motion, for motion along $\hat{\mathbf{u}}_1$, $\hat{\mathbf{u}}_2$, and $\hat{\mathbf{u}}_3$, respectively (note that in our simulations we do not really move the particles). The mixing term ξ' represents friction along the $\hat{\mathbf{u}}_1$ direction for motion along the $\hat{\mathbf{u}}_3$ direction (and vice versa). The mixing term is always found to be at least one order of magnitude smaller than the three diagonal components, so to a first approximation may be neglected. The fact that the mixing term is always much smaller than the diagonal components shows that $\hat{\mathbf{u}}_1$, $\hat{\mathbf{u}}_2$, and $\hat{\mathbf{u}}_3$ are indeed close to the principal axes of the friction tensor. Moreover, the convergence of the friction data was confirmed by performing duplo runs for

Downloaded 21 Oct 2011 to 131.155.151.93. Redistribution subject to AIP license or copyright; see http://jcp.aip.org/about/rights_and_permissions

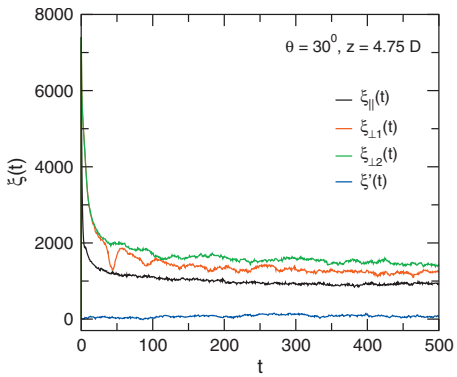

FIG. 4. Running integral of the autocorrelation of the constraint force needed to keep a rod at fixed position $Z=4.75D$ and orientation $\theta=30^0$. The diagonal components represent the magnitude of the friction antiparallel to the direction of "motion," for motion along $\hat{\mathbf{u}}_1$ ($\xi_\parallel$), $\hat{\mathbf{u}}_2$ ($\xi_{\perp 1}$), and $\hat{\mathbf{u}}_3$ ($\xi_{\perp 2}$). The mixing term ξ' represents friction along the $\hat{\mathbf{u}}_1$ direction for motion along the $\hat{\mathbf{u}}_3$ direction (and vice versa). The mixing term is always much smaller than the diagonal components.

most systems, yielding identical results (including, for example, the oscillation visible in $\xi_{\perp 1}(t)$ near $t=50t_0$).

The Enskog friction was again determined from the peak value of the running integral at short times and the total friction from the limiting value at large times. The resulting hydrodynamic frictions are presented in Fig. 5 (symbols) as a function of distance between rod and wall for four values of the angle θ. We find that a reasonable approximation (within the range of distances studied) for the translational friction components is to treat the wall effect as additional to the bulk friction, with a dominant dependence on the inverse smallest distance between the surface of the rod and the wall and an angle-dependent prefactor. The smallest distance is defined as follows: a shish-kebab rod consisting of L/D spheres, with its center-of-mass at height $z=Z$, making an angle θ with the wall normal, will have a smallest distance d_1 with the wall at $z=0$ given by

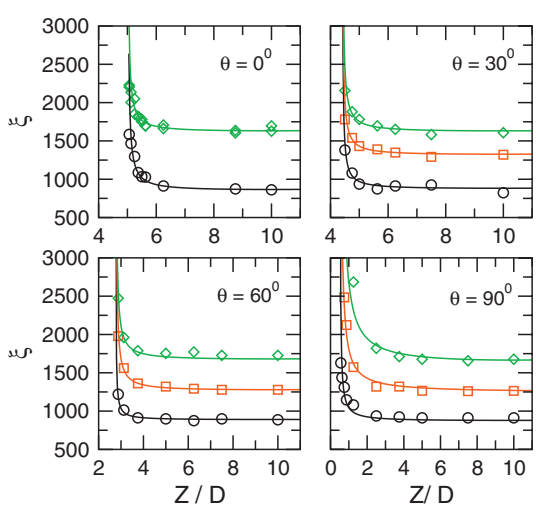

FIG. 5. Hydrodynamic translational friction components $\xi_\parallel$ (black circles), $\xi_{\perp 1}$ (red squares), and $\xi_{\perp 2}$ (green diamonds) as a function of rod height Z, for four different angles θ. Solid lines are fits using Eq. (20).

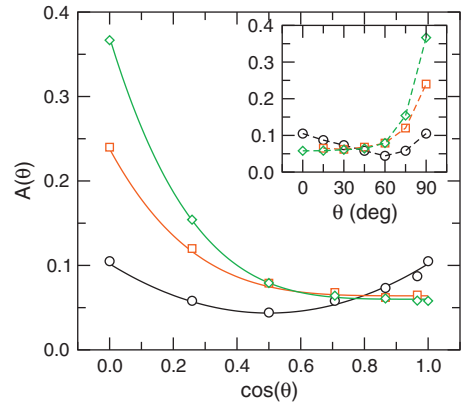

FIG. 6. Prefactors $A_\parallel(\theta)$ (black circles), $A_{\perp 1}(\theta)$ (red squares), and $A_{\perp 2}(\theta)$ (green diamonds), as obtained from fits to translational friction coefficients using Eq. (20), vs rod angle θ (inset) or cos θ (main plot). Solid lines in the main plot are fits using Eqs. (21)–(23).

$$d_1 = Z - \left[\frac{L/D-1}{2}\cos\theta + \frac{1}{2}\right]D. \tag{19}$$

Another wall is present at $z=L_z$, with a smallest distance d_2 to the surface of the rod given by $d_2=L_z+d_1-2Z$. Within our approximation, the translational friction components may be expressed as

$$\xi_{\alpha\beta} \approx \xi_{\alpha\beta}^{\infty}\left[1 + A_{\alpha\beta}(\theta)\left(\frac{D}{d_1}+\frac{D}{d_2}\right)\right], \tag{20}$$

where $\xi_{\alpha\beta}$ can be any of the $\xi_\parallel$, $\xi_{\perp 1}$, or $\xi_{\perp 2}$ components. The fits are presented in Fig. 5 as solid lines. The $z=\infty$ values and prefactors A are estimated by a least-squares fit. Note that the prefactors A may in principle also depend on the aspect ratio $p=L/D$. Our results apply to the case $p=10$ only. We find the following results for the bulk values (in our units): $\xi_\parallel^\infty = 860\pm 20$, $\xi_{\perp 1}^\infty = 1250\pm 50$, and $\xi_{\perp 2}^\infty = 1500\pm 80$, independent of the particular value of θ. These values may be compared to the approximate theoretical predictions[37] $\xi_\parallel^{\text{theor}} = 2\pi\eta L/(\ln p - 0.207 + 0.908/p) = 575$ and $\xi_\perp^{\text{theor}} = 4\pi\eta L/(\ln p + 0.839 + 0.185/p) = 800$ valid for a cylindrical rod in an infinite solvent bath. The frictions we measure are higher because of unavoidable self-interactions between the rod and its periodic images, which overall tend to increase the friction. In other words, even when the walls are infinitely far apart (in the z-direction), the periodic boundaries in the other two directions still cause friction enhancements of each of the friction components. We find that the self-interactions enhance the component $\xi_\parallel^\infty$ by the same amount, independent of the actual rod angle θ. Similarly the values for $\xi_{\perp 1}^\infty$ and $\xi_{\perp 2}^\infty$ are consistently the same for all rod angles.

In Fig. 6 (inset), we present the prefactors A, as obtained from the fits, as a function of rod angle θ. In the absence of theoretical predictions, we have tried several fit functions. Good single power law fits can be made when the prefactors are plotted against cos θ, see Fig. 6 (main plot), resulting in the following fit functions:

$$A_\parallel(\theta) = A_\parallel^0 + B_\parallel(1/2 - \cos\theta)^2, \tag{21}$$

$$A_{\perp 1}(\theta) = A_{\perp 1}^0 + B_{\perp 1}(1 - \cos\theta)^4, \tag{22}$$

Downloaded 21 Oct 2011 to 131.155.151.93. Redistribution subject to AIP license or copyright; see http://jcp.aip.org/about/rights_and_permissions

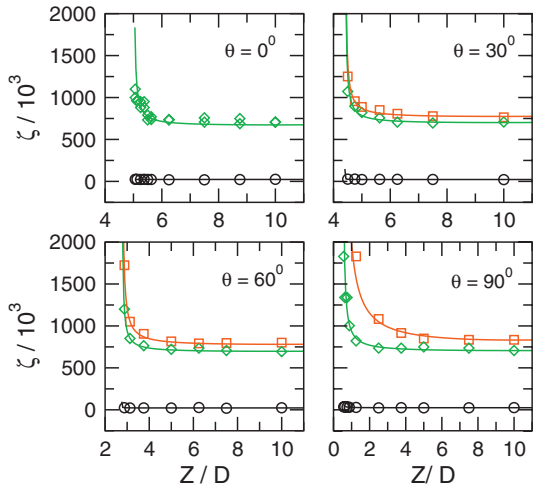

FIG. 7. Hydrodynamic rotational friction components $\zeta_{\parallel}$ (black circles), $\zeta_{\perp 1}$ (red squares) and $\zeta_{\perp 2}$ (green diamonds) as a function of rod height Z, for four different angles θ. Solid lines are fits using Eq. (27).

$$A_{\perp 2}(\theta) = A^0_{\perp 2} + B_{\perp 2}(1 - \cos\theta)^4, \tag{23}$$

with $A^0_{\parallel} = 0.044 \pm 0.003$, $B_{\parallel} = 0.23 \pm 0.02$, $A^0_{\perp 1} = 0.064 \pm 0.005$, $B_{\perp 1} = 0.17 \pm 0.02$, $A^0_{\perp 2} = 0.060 \pm 0.004$, and $B_{\perp 2} = 0.31 \pm 0.02$.

In summary, if only one wall is present near a rod of $L/D = 10$ with closest distance d, the translational friction components are approximately given by

$$\xi_{\parallel} \approx \xi^{\infty}_{\parallel}\left\{1 + [0.044 + 0.23(1/2 - \cos\theta)^2]\frac{D}{d}\right\}, \tag{24}$$

$$\xi_{\perp 1} \approx \xi^{\infty}_{\perp}\left\{1 + [0.064 + 0.17(1 - \cos\theta)^4]\frac{D}{d}\right\}, \tag{25}$$

$$\xi_{\perp 2} \approx \xi^{\infty}_{\perp}\left\{1 + [0.060 + 0.31(1 - \cos\theta)^4]\frac{D}{d}\right\}. \tag{26}$$

B. Rotational friction

Figure 7 (symbols) shows the hydrodynamic rotational friction coefficients as a function of distance between rod and wall for four different values of the angle θ. The component $\zeta_{\parallel}$ (circles) represents the rotational friction for rotation around the long ($\hat{\mathbf{u}}_1$) axis, $\zeta_{\perp 1}$ represents the rotational friction for rotation around the $\hat{\mathbf{u}}_2$ axis, and $\zeta_{\perp 2}$ the rotational friction for rotation around the $\hat{\mathbf{u}}_3$ axis. The mixing term ζ' was again found to be at least one order of magnitude smaller and is therefore neglected in the following analysis.

Similarly to the translational friction, we have treated the wall effect as additive to the bulk rotational friction, again with a dominant inverse dependence on the smallest distance d. Denoting rotational friction components with ζ, these may be expressed as

$$\zeta_{\alpha\beta} \approx \zeta^{\infty}_{\alpha\beta}\left[1 + C_{\alpha\beta}(\theta)\left(\frac{D}{d_1} + \frac{D}{d_2}\right)\right], \tag{27}$$

where $\zeta_{\alpha\beta}$ can be any of the $\zeta_{\parallel}$, $\zeta_{\perp 1}$, or $\zeta_{\perp 2}$ components. The fits are represented in Fig. 7 as solid lines. Again note that

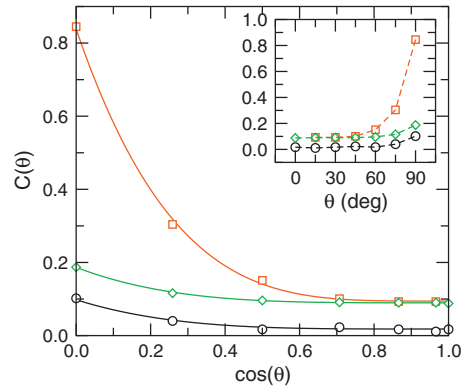

FIG. 8. Prefactors $C_{\parallel}(\theta)$ (black circles), $C_{\perp 1}(\theta)$ (red squares), and $C_{\perp 2}(\theta)$ (green diamonds), as obtained from fits to rotational friction coefficients using Eq. (27), vs rod angle θ (inset) or $\cos\theta$ (main plot). Solid lines in the main plot are fits using Eqs. (28)–(30).

the prefactors C may also depend on the aspect ratio $p = L/D$. We find the following values for the bulk values (in our units): $\zeta^{\infty}_{\parallel} = (0.22 \pm 0.01) \times 10^5$, $\zeta_{\perp 1} = (7.4 \pm 0.1) \times 10^5$, and $\zeta_{\perp 2} = (6.7 \pm 0.2) \times 10^5$. Theoretically, the expression for a cylindrical rod of aspect ratio $p = 10$ for the latter two reads[37] $\zeta^{\text{theor}}_{\perp} = \pi\eta L^3/[3(\ln p - 0.662 + 0.917/p)] = 7.7 \times 10^5$. We consider the rather good agreement with our results to be somewhat fortuitous: the theoretical results have been derived for a cylinder of length L and diameter D in an infinite bath, whereas we have simulated a succession of spheres in a finite bath. Because forces on the extremes of a rod have the most important contribution to the torque, the magnitude of the rotational friction on a rod is much more sensitive to the shape of its extremes than the translational friction. The rounded extremes of our model would correspond effectively to a cylinder of smaller length (for example for a cylinder with $L = 9D$ a rotational friction of $\zeta_{\perp} = 6.0 \times 10^5$ would be predicted).

The rotational friction around the long axis is less than 3% of those around the two perpendicular axes, and relatively it remains much smaller also when the distance to a wall becomes very small. In Fig. 8 (inset), we present the prefactors C, as obtained from the fits, as a function of rod angle θ. Good single power law fits can again be made with our measurements when they are plotted against $\cos\theta$ (main plot), resulting in the following fit functions:

$$C_{\parallel}(\theta) = C^0_{\parallel} + E_{\parallel}(1 - \cos\theta)^4, \tag{28}$$

$$C_{\perp 1}(\theta) = C^0_{\perp 1} + E_{\perp 1}(1 - \cos\theta)^4, \tag{29}$$

$$C_{\perp 2}(\theta) = C^0_{\perp 2} + E_{\perp 2}(1 - \cos\theta)^4, \tag{30}$$

with $C^0_{\parallel} = 0.036 \pm 0.002$, $E_{\parallel} = 0.080 \pm 0.006$, $C^0_{\perp 1} = 0.094 \pm 0.004$, $E_{\perp 1} = 0.74 \pm 0.04$, $C^0_{\perp 2} = 0.090 \pm 0.004$, and $E_{\perp 2} = 0.097 \pm 0.005$. In summary, if one wall is present near a rod of $L/D = 10$ with closest distance d, the rotational friction components are approximately given by

$$\zeta_{\parallel} \approx \zeta^{\infty}_{\parallel}\left\{1 + [0.036 + 0.08(1 - \cos\theta)^4]\frac{D}{d}\right\}, \tag{31}$$

Downloaded 21 Oct 2011 to 131.155.151.93. Redistribution subject to AIP license or copyright; see http://jcp.aip.org/about/rights_and_permissions

$$\zeta_{\perp 1} \approx \zeta_{\perp}^{\infty}\left\{1 + [0.094 + 0.74(1 - \cos\theta)^4]\frac{D}{d}\right\}, \tag{32}$$

$$\zeta_{\perp 2} \approx \zeta_{\perp}^{\infty}\left\{1 + [0.090 + 0.097(1 - \cos\theta)^4]\frac{D}{d}\right\}, \tag{33}$$

V. CONCLUSION

We have shown that SRD simulations can be used to measure the hydrodynamic friction on an object by constraining its position and orientation and analyzing the time correlation of the constraint force.

In this work, we have applied the method to a rod of aspect ratio $L/D=10$ near a wall. The main result is summarized in Eqs. (24)–(26) and (31)–(33). Reasonably good fits of both the translational and rotational friction could be made with the inverse of the closest distance d between the rod and wall, at least in the range $d \in [D/8, L]$.

We have found that for a noticeable friction increase the closest distance between rod and wall needs to be on the order of the rod diameter. Also, in agreement with common sense, the friction increase is strongest when the rod lies parallel to the wall ($\cos\theta=0$). For translations, the friction component $\xi_{\perp 2}$ is the largest, as this corresponds (at least partially) to motion to and from the wall. For rotations, the friction component $\zeta_{\perp 1}$ is the largest, as this corresponds to motion to and from the wall of the extremities of the rod.

In anticipation of an accurate theoretical treatment of this system, we have fitted the angular dependence of the friction components and found good fits in most cases with $(1-\cos\theta)^4$. We do not have a motivation for this functional form except that, intuitively, the friction increase must be relatively larger when a larger area of the rod is exposed close to the wall. Hence an increasing function of angle θ is expected. The only exception seems to be the angular dependence of the parallel translational friction $\xi_{\parallel}$, for which the smallest friction increase occurs at an intermediate angle of 60° (see the inset of Fig. 6). Because we cannot give a full physical motivation, the scalings we have presented here are possibly not exact. However, they do serve to represent our measurements in a compact form which may be useful for future simulations. Such simulations are planned for the near future.

More generally, the technique presented in this paper offers the possibility to determine with reasonable precision the hydrodynamic frictions on complex objects, possibly with nearby complex boundaries, under circumstances where theoretical calculations are too difficult to be performed.

ACKNOWLEDGMENTS

We thank Peter Lang and Jan Dhont for useful discussions. We thank the NoE "SoftComp" and NMP SMALL "Nanodirect" for financial support. J.T.P. thanks the Netherlands Organisation for Scientific Research (NWO) for additional financial support.

[1] H. Faxén, Ark. Mat., Astron. Fys. **17**, 1 (1923).
[2] H. Brenner, Chem. Eng. Sci. **16**, 242 (1961).
[3] H. Brenner, J. Fluid Mech. **12**, 35 (1962).
[4] T. S. Squires and S. R. Quake, Rev. Mod. Phys. **77**, 977 (2005).
[5] J. K. G. Dhont, *An Introduction to the Dynamics of Colloids* (Elsevier, Amsterdam, 1996).
[6] V. N. Michailidou, G. Petekidis, J. W. Swan, and J. F. Brady, Phys. Rev. Lett. **102**, 068302 (2009).
[7] A. J. Goldman, R. G. Cox, and H. Brenner, Chem. Eng. Sci. **22**, 637 (1967).
[8] R. G. Cox and H. Brenner, J. Fluid Mech. **28**, 391 (1967).
[9] K. D. Kihm, A. Banerjee, C. K. Choi, and T. Tagaki, Exp. Fluids **37**, 811 (2004).
[10] A. Banerjee and A. D. Kihm, Phys. Rev. E **72**, 042101 (2005).
[11] M. D. Carbajal-Tinoco, R. Lopez-Fernandez, and J. L. Arauz-Lara, Phys. Rev. Lett. **99**, 138303 (2007).
[12] K. Zahn, R. Lenke, and G. Maret, J. Phys. II **4**, 555 (1994).
[13] M. A. Bevan and D. C. Prieve, J. Chem. Phys. **113**, 1228 (2000).
[14] P. Huang and K. S. Breuer, Phys. Rev. E **76**, 046307 (2007).
[15] P. Holmqvist, J. K. G. Dhont, and P. R. Lang, Phys. Rev. E **74**, 021402 (2006).
[16] P. Holmqvist, J. K. G. Dhont, and P. R. Lang, J. Chem. Phys. **126**, 044707 (2007).
[17] L. J. Durlofsky and J. F. Brady, J. Fluid Mech. **200**, 39 (1989).
[18] G. Bossis, A. Meunier, and J. D. Sherwood, Phys. Fluids A **3**, 1853 (1991).
[19] A. Meunier, J. Phys. II **4**, 561 (1994).
[20] J. W. Swan and J. F. Brady, Phys. Fluids **19**, 113306 (2007).
[21] B. Cichocki, R. B. Jones, R. Kutteh, and E. Wajnryb, J. Chem. Phys. **112**, 2548 (2000); B. Cichocki, M. L. Ekiel-Jezewska, G. Nägele, and E. Wajnryb, *ibid.* **121**, 2305 (2004); B. Cichocki, M. L. Ekiel-Jezewska, and E. Wajnryb, *ibid.* **126**, 184704 (2007).
[22] M. L. Ekiel-Jeżewska, K. Sadlej, and E. Wajnryb, J. Chem. Phys. **129**, 041104 (2008).
[23] A. Malevanets and R. Kapral, J. Chem. Phys. **110**, 8605 (1999).
[24] A. Malevanets and R. Kapral, J. Chem. Phys. **112**, 7260 (2000).
[25] J. T. Padding, A. Wysocki, H. Löwen, and A. A. Louis, J. Phys.: Condens. Matter **17**, S3393 (2005).
[26] J. T. Padding and A. A. Louis, Phys. Rev. E **74**, 031402 (2006).
[27] N. Kikuchi, N. Pooley, C. M. Ryder, and J. M. Yeomans, J. Chem. Phys. **119**, 6388 (2003).
[28] T. Ihle, E. Tüzel and D. M. Kroll, Phys. Rev. E **70**, 035701(R) (2004).
[29] R. L. C. Akkermans and W. J. Briels, J. Chem. Phys. **113**, 6409 (2000).
[30] J. T. Padding and W. J. Briels, J. Chem. Phys. **117**, 925 (2002).
[31] J. T. Hynes, Annu. Rev. Phys. Chem. **28**, 301 (1977).
[32] J. T. Hynes, R. Kapral, and M. Weinberg, J. Chem. Phys. **70**, 1456 (1979).
[33] S. H. Lee and R. Kapral, J. Chem. Phys. **121**, 11163 (2004).
[34] A. A. Zick and G. M. Homsy, J. Fluid Mech. **115**, 13 (1982).
[35] B. Dünweg and K. Kremer, J. Chem. Phys. **99**, 6983 (1993).
[36] T. Ihle and D. M. Kroll, Phys. Rev. E **63**, 020201(R) (2001).
[37] M. M. Tirado, C. L. Martínez, and J. G. de la Torre, J. Chem. Phys. **81**, 2047 (1984).

Downloaded 21 Oct 2011 to 131.155.151.93. Redistribution subject to AIP license or copyright; see http://jcp.aip.org/about/rights_and_permissions